



## Photocatalytic Degradation of Reactive Black 5 Using Photo-Fenton and ZnO Nanoparticles under UV Irradiation



Mohamed A. Hassaan<sup>1\*</sup>, Marwa R. Elkatory<sup>2</sup>, Rehab M. Ali<sup>3</sup>, Ahmed El Nembr<sup>1</sup>

<sup>1</sup>Marine Environmental Division, National Institute of Oceanography and Fisheries, Alexandria, Egypt.

<sup>2</sup>Advanced Technology and New Materials Research Institute, City of Scientific Research and Technological Applications (SRTA-City), Alexandria 21934, Egypt.

<sup>3</sup>Fabrication Technology Department, Advanced Technology and New Materials and Research Institute (ATNMRI), City of Scientific Research and Technological Applications (SRTA-City), Alexandria, Egypt.

**D**UE to their extensive range of applications, the existence of notable amounts of reactive dyes in wastewater raises the need for more efficient treatment techniques. The present work investigates the removal of Reactive Black 5 (RB5) azo dye by homogeneous advanced oxidation processes (photo-Fenton) and heterogeneous advanced oxidation processes (ZnO nanoparticle / UV). The Synthesized ZnO nanoparticles (NPs) were characterized using Fourier transforms infrared (FTIR), transmission electron microscopy (TEM), Scanning electron microscope (SEM), X-ray diffraction (XRD), UV-Vis spectroscopy, and the photoluminescence (PL). The formation of ZnO NPs was confirmed by FTIR with a broad band at 420.50 cm<sup>-1</sup>. TEM analysis shows that the synthesized ZnO NPs particle size ranged between 19.1 and 33.1 nm. The ZnO NPs hexagonal phase was observed from XRD analysis. Photo-Fenton (FeSO<sub>4</sub>·7H<sub>2</sub>O/ UV/H<sub>2</sub>O<sub>2</sub>) showed high decolorization rate of RB5 reached 98% within the first 5 min. While ZnO NPs showed lower decolorization rate during the same period. The effects of FeSO<sub>4</sub>·7H<sub>2</sub>O initial dosage, RB5 initial concentrations, ZnO initial dosage and contact time were investigated as well.

**Keywords:** Photo-Fenton, Advanced oxidation, ZnO nanoparticles, Reactive black 5, Dye degradation

### Introduction

The textile industries produce about 60 x 10<sup>6</sup> tons of fabrics and consume about (35 x 10<sup>9</sup>) tons of water during manufacturing processes every year. In general, the wastewater from textile industry contains considerable amounts of few or non-biodegradable materials such as volatile organic compounds, dyes, ethylene, etc. [1-5]. Currently, a lot of techniques used for wastewater treatment including chemical oxidation, adsorption, biological and biochemical methods and many other techniques [6-8]. The above mentioned techniques may be suitable for one or more pollutants as a part of their advantages and disadvantages. Therefore, there is a demand

for improvement of method that is greatly selective, easy to handle and economical for each dye. Specific reactive dyes make considerable problems due to their non-biodegradable compounds. Advanced oxidation processes (AOPs), have been used for the degradation of reactive dyes, [9-12]. AOPs generate hydroxyl radicals (·OH) that react with organic compounds (dyes) to create innocuous products such as H<sub>2</sub>O, CO<sub>2</sub>, and other intermediate products throughout the degradation process. The photo-Fenton process including H<sub>2</sub>O<sub>2</sub>, FeSO<sub>4</sub> and UV radiation takes short reaction times among the AOPs [13-15].

The reactions of photo-Fenton are shown in

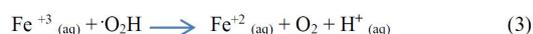
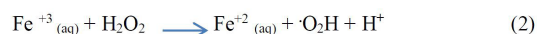
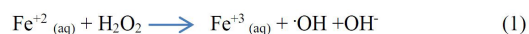
\*Corresponding author e-mail: mhss95@mail.com.Tel. 0020121199123

Received 08/08/2019; Accepted 17/09/2019

DOI: [10.21608/ejchem.2019.15799.1955](https://doi.org/10.21608/ejchem.2019.15799.1955)

©2020 National Information and Documentation Center (NIDOC)

Eqs. 1-4 [16, 17]:



This process is appropriate due to complete degradation of reactive dyes, high decolorization rate, efficiency and decline of lethal chemicals [18–22], organic materials [23], pesticides [24], herbicides [25], and pharmaceutical impurities [26–28].

The objectives of this study can be listed as the following:

1- Synthesis and characterization of ZnO NPs using FTIR, SEM, TEM, XRD, UV-vis spectroscopy and PL.

2- Studying the effect of the initial catalyst dose of both ZnO NPs and  $\text{FeSO}_4 \cdot 7\text{H}_2\text{O}$  on the degradation of RB5 dye

3- Studying the effect of the optimal catalyst dose on the different initial RB5 dye concentrations and its proposed degradation mechanism using both ZnO NPs and photo-Fenton.

## Materials and Methods

RB5 was supplied from ISMA dye company Kafer Eldawar, Egypt ~ 75% of dye content and used without additional purification.  $\text{FeSO}_4 \cdot 7\text{H}_2\text{O}$  (Merck) and  $\text{H}_2\text{O}_2$  (Merck, 35% w/w) were used as reagent grade. RB5 chemical structure is shown in Fig. 1. A stock solution of 1,000 mg/L of RB5 was prepared using double distilled water (DDW). Other aqueous solutions of RB5 (50, 75, 100, 125 and 200 mg/L) were prepared from the stock solution by dilution with DDW to the prerequisite concentrations. UV-vis spectrophotometer (Model No 45600-02, Cole Parmer Instrument Co., USA) was employed for absorbance measurements. The maximum wavelength  $\lambda_{\text{max}}$  for RB5 was determined at 597 nm. The color removal rate of RB5 was calculated following Eq. 5.

$$\% \text{ Removal} = \frac{A_0 - A_t}{A_0} \times 100 \quad (5)$$

Where  $A_0$  and  $A_t$  are the initial and the measured absorbance of the samples at different time intervals.

*Egypt. J. Chem.* Vol. 63, No. 4 (2020)

## UV based AOPs

Batch experiments, for photo-Fenton oxidation, were implemented in a Horizontal laminar flow cabinet (Bw-LFH1300) with 254 nm UV mercury lamp of 30 W power, as shown in Fig. 2. The cylindrical reactor of 500 mL capacity was made of glass. For every experiment achievement, the reactor was initially loaded with 200 mL of RB5 aqueous solution (100 mg/L) and the mixing was continued by means of a magnetic stirrer. In case of utilizing  $\text{FeSO}_4 \cdot 7\text{H}_2\text{O}/\text{UV}/\text{H}_2\text{O}_2$ , 1 ml of  $\text{H}_2\text{O}_2$  (35% w/w) was added to each sample in the photoreactor and was irradiated by UV dose of 30 W with continuous stirring at 200 rpm. Firstly, the  $\text{H}_2\text{O}_2$  was added to the dye solution and then the pH was adjusted to the desired value by the addition of a few drops of either  $\text{H}_2\text{SO}_4$  or NaOH. In the case of utilizing ZnO NPs / UV, the same procedures were followed. The initial pH was set at 7 with 1 M  $\text{H}_2\text{SO}_4$  or 1 M NaOH before starting different AOPs processes. The pH measurements were carried out using JENCO Electronics, LTD pH meter.

## ZnO synthesis and characterization

### Synthesis of ZnO NPs

To 100 ml of DDW, a 0.4 g portion of zinc acetate dihydrate ( $\text{Zn}(\text{CH}_3\text{CO}_2)_2 \cdot 2\text{H}_2\text{O}$ ) was added under vigorous stirring for 10 min. The pH of the solution was dropwise adjusted by the addition of 0.1 M NaOH until the pH became 12. The mixture was stirred for 2-3 h and the obtained pale white precipitate was separated, washed many times with DDW and ethanol then left to dry at 80°C under vacuum overnight. For the attainment of pure ZnO NPs, the obtained product was calcinated at 550°C for 4 hours.

### Characterization of Structural Properties of ZnO NPs

#### Fourier transforms infrared (FTIR)

The properties of ZnO NPs were investigated by Fourier transform infrared spectroscopy (FTIR) analysis. The characterization involved the analysis of the dried powder of the synthesized ZnO nanoparticles confirmed by using (IRAffinity-1SFTIR spectrometer Shimadzu, Japan). The spectra (128 scans at 2  $\text{cm}^{-1}$  resolution) were collected with the frequency range of 4000-400  $\text{cm}^{-1}$ , with a resolution enhancement factor of 1.5 and a bandwidth of 15  $\text{cm}^{-1}$ .

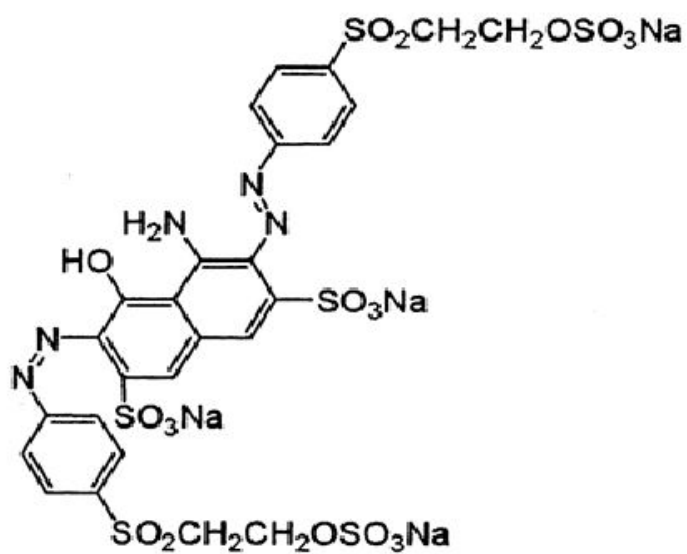


Fig.1. Chemical structure of RB5 (Molecular Formula:  $C_{26}H_{21}N_5Na_4O_{19}S_6$ ) (Molecular Weight: 991.82).  $\lambda_{Max} = 597\text{nm}$ ; C.I.20505.

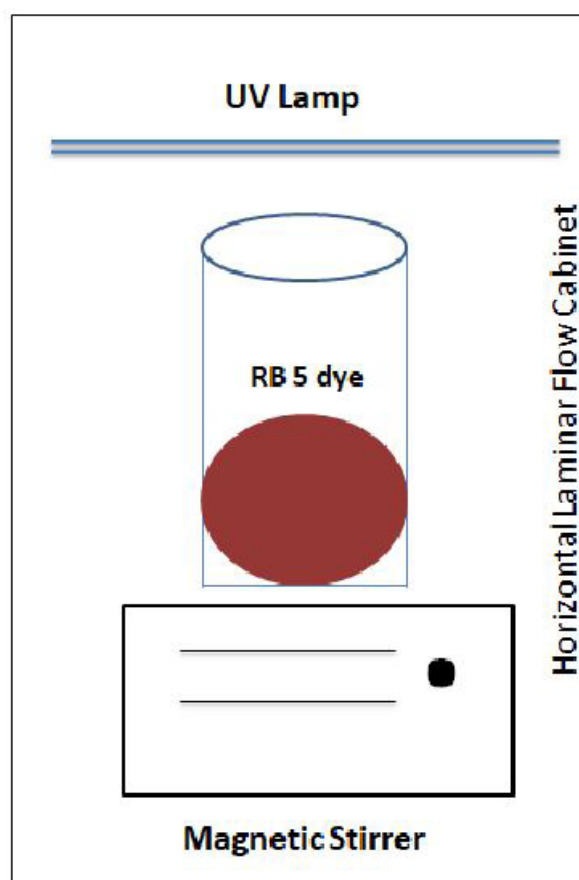


Fig.2. Schematic diagram of Photocatalytic test

### Scanning electron microscope (SEM)

The morphology and surface features were characterized by scanning electron microscope (SEM- JEOL JSM 6360LA, Japan). SEM analysis was carried out at room temperature with an accelerating voltage of 20 kV.

### Transmission electron microscopy (TEM)

The average size and the structure of ZnO NPs were determined by transmission electron microscopy (TEM), (TEM; Tecnai™ G2 Spirit, FEI), operated at a high voltage range of 20–120 kV/ LaB6 TEM.

### X-ray Diffraction (XRD)

The crystalline phase of ZnO powders was analyzed by X-ray diffraction (XRD) using a (Shimadzu XRD-7000 diffractometer, Japan). The operation conditions at 40 kV and 30 mA were used with Cu K $\alpha$ , Ni-filtered radiation ( $\lambda = 1.5418 \text{ \AA}$ ) and  $2\theta$  ranging from 5 to 80°.

### UV-vis spectroscopy

The sample was measured for its maximum absorbance using UV-vis spectrophotometry. The optical properties of the prepared ZnO NPs were characterized using a (LAMBDA 650 UV/Vis Spectrophotometer) in the range of 200–600 nm.

### The photoluminescence (PL)

The photoluminescence (PL) data were recorded using a xenon flash lamp at an excitation wavelength of 330 nm. The reflectance spectra were collected using a (Cary Eclipse fluorescence spectrophotometer). All measurements were done at room temperature.

## Results and Discussion

### ZnO characterization

#### FTIR

From Fig. 3, there is a broad band at 420.50  $\text{cm}^{-1}$  which is corresponding to the E2 mode of the hexagonal ZnO (Raman active), [29-31]. The band around 889.21  $\text{cm}^{-1}$  agrees with [32] who observed ZnO absorption stretching band around 887  $\text{cm}^{-1}$ . A series of bands from 1000 to 4000  $\text{cm}^{-1}$  can be found, which correspond to the carboxylate and hydroxyl impurities in the materials. More in detail, the broad band at 3458.48  $\text{cm}^{-1}$  was assigned to the O-H stretching

mode of the OH group [30].

#### SEM

The major features of the physical surface structure of ZnO NPs were shown in Fig. 4. It can be observed that the surface is compacted and rough with an irregular lumpy shape which may increase the area of contact. In addition, the surface contains many pores that can provide a large surface for RB5 degradation.

#### TEM

The nanoparticles distribution and morphology were further characterized using TEM analysis as shown in Fig. 5. The synthesized ZnO NPs particle size ranged between 19.1 nm and 33.1 nm. The TEM images demonstrate the internal structure of the nanoparticles and provide more accuracy on their size. All the TEM characterization was carried out one day after the preparation process.

#### XRD

All the obtained peaks in the XRD pattern of as-grown nanoparticles are similar to known wurtzite-structured hexagonal phase single crystalline bulk ZnO (**JCPDS Card No. 89-1397**) confirming the synthesis of pure ZnO NPs. The peaks are shown in Fig. 6, with  $2\theta$  values of 31.67°, 34.31°, 36.15°, 47.46°, 56.54°, 62.79°, 66.34°, 67.89°, 69.02°, and 76.89° correspond to the crystal planes of (100), (002), (101), (102), (110), (103), (200), (112), (201) and (202), respectively.

The crystallite sizes of the ZnO NPs (Table 1) were estimated from full-width at half-maximum of the 101 anatase peak by the Debye-Scherrer Eq.(6) [33,43]

$$Cs = 0.89\lambda/\beta\cos\theta \quad (6)$$

Where  $Cs$ ,  $\lambda$ ,  $\theta$ , and  $\beta$  indicate the crystallite size, the X-ray wavelength (1.5406 $\text{\AA}$ ), Bragg diffraction angle corresponding to the (101) plane, and full width at half maximum (FWHM) of the (101) plane, respectively.

The Scherrer formula was used to calculate the crystallite sizes and was found to be in the range of 2.5–3.6 nm. XRD study confirmed the presence of even smaller particles than the TEM examination. The larger nanoparticles of ZnO (about 33.1 nm) in the sample result from the agglomeration of smaller nanoparticles, whose

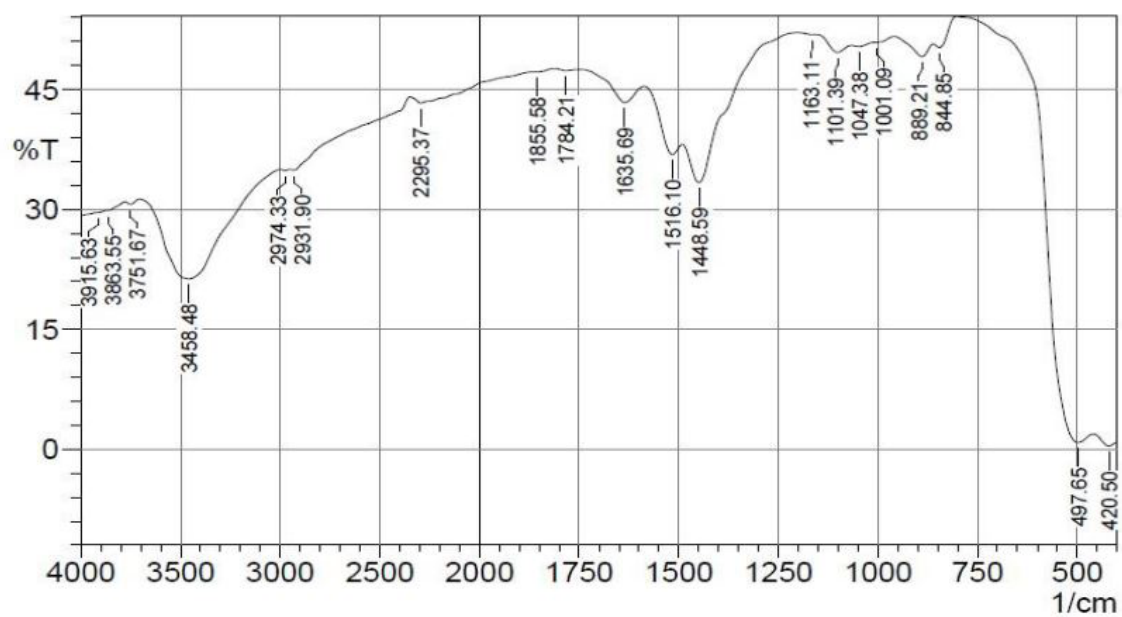


Fig.3. FTIR spectrum of chemically synthesized ZnO NPs.

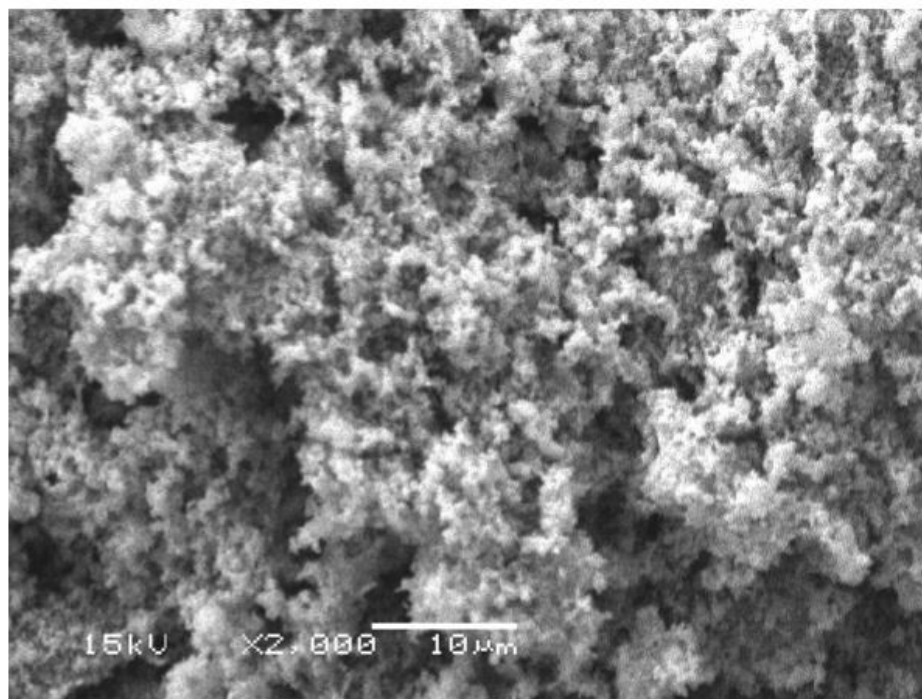


Fig. 4. SEM image of chemically synthesized ZnO NPs

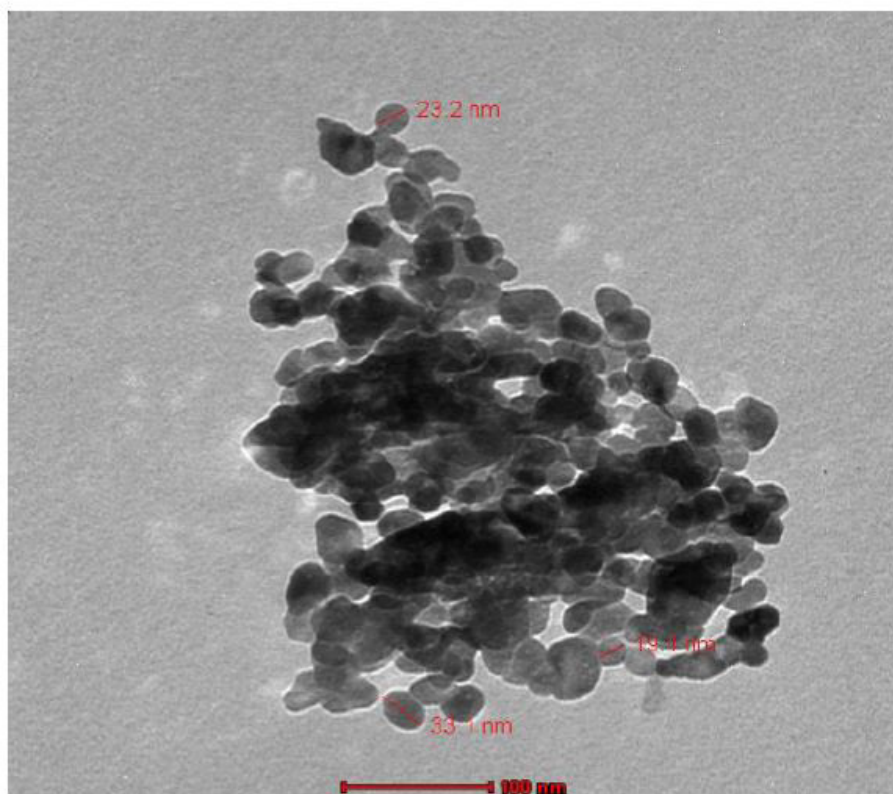


Fig. 5. TEM image of chemically synthesized ZnO NPs

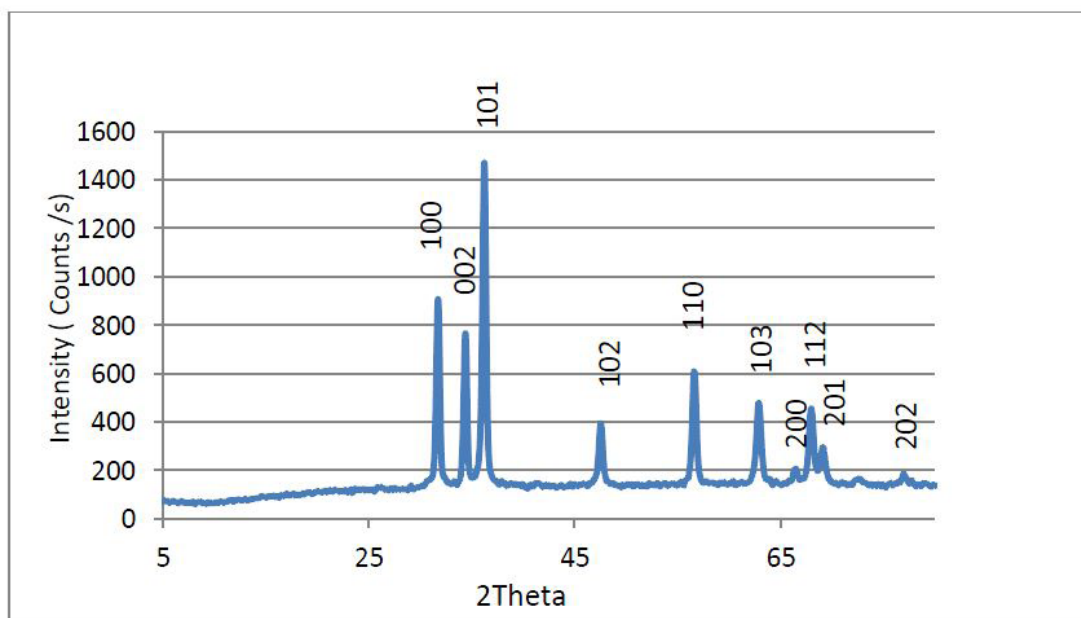


Fig.6. XRD spectra of chemically synthesized ZnO NPs

presence is confirmed by XRD [35]. The XRD method allowed for the identification of smaller sizes of nanoparticles [35].

#### *UV-vis*

Figure 7 shows the UV-vis absorbance spectrum of ZnO nanostructures suspended in ethanol. A strong and sharp peak presents at 380.49 nm which corresponds to the band gap of 3.25 eV and is in good agreement with reported literature confirming the synthesis of ZnO [36, 37]. The band gap ( $E$ , eV) of the samples was calculated by using Eq. (7) [38] as follows:

$$E = 1240/\lambda_{\max} \quad (7)$$

where  $\lambda_{\max}$  is the wavelength at the maximum absorption.

#### *Photoluminescence*

The photoluminescence (PL) spectra of the ZnO NPs have been measured at an excitation wavelength of 330 nm as shown in Fig. 8. Chemical synthesized ZnO NPs showed two broad and asymmetric band in the visible region located at 385.8 and 661.8 nm which is ascribed to the band to band and defect transitions in ZnO, respectively [39-41]. The emission band at 661.8 nm may be due to doubly ionized oxygen ( $\text{Vo}^-$ ) vacancies, [41].

#### *Optimization of ZnO NPs for the RB5 degradation*

The effect of ZnO NPs dose on the RB5 degradation was tested using 0.1, 0.2, 0.4, 0.8 and 1 g ZnO NPs / 200 mL of RB5 dye solution of 100 mg/L for 1 h. The experiments were performed in the presence of  $\text{H}_2\text{O}_2$  35% by adding 1 mL of it to the solution, then the RB5 dye solution was separated by centrifuge to determine the rest RB5 dye concentrations.

The effect of ZnO NPs dose on RB5 degradation process was represented in Fig. 9a which shows that the removal efficiency of RB5 dye was decreased from 87.92 to 23.47% by increasing the ZnO NPs dose from 0.1 to 1g. These results agree with Shahab-ud-Din et al. [42] who degraded (photo-catalytically) CR-F3BS dye under UV light as function of catalyst dosage and it was revealed the maximum CR-F3BS degradation of 94.3% was achieved at 0.275 g/L catalyst dose and the percentage of dye removal was declined to 79% by increasing the catalyst ( $\alpha$ -MoO<sub>3</sub> micro-belts) dose to 2 g/L. The same

trend of low catalyst dose is also mentioned by some other literature [43-45].

Time is another effective parameter for RB5 degradation processes. Increasing time increases the RB5 dye degradation to reach 90 % after the first 1h of photocatalytic process. The color removal efficiency reached 24% during the first 5 minutes for 0.1 g of ZnO NPs as seen in Fig. 9b. From the abovementioned results, the optimum ZnO NPs dose is 0.1 g. The results revealed that the degradation rate depends on the ZnO dose which follows comparable results reported by [43].

#### *Optimization of FeSO<sub>4</sub>.7H<sub>2</sub>O for the RB5 degradation*

The effect of FeSO<sub>4</sub>.7H<sub>2</sub>O dose on the RB5 degradation was tested using 0.1, 0.2, 0.4, 0.8 and 1 g FeSO<sub>4</sub>.7H<sub>2</sub>O /200 mL of RB5 dye solution of 100 mg/L for 30 min. The experiments were performed same as in ZnO NPs.

The effect of FeSO<sub>4</sub>.7H<sub>2</sub>O dose on the RB5 degradation process was represented in Fig. 10a which shows that the removal efficiency of RB5 dye was decreased from 99.84 to 93.92 % by increasing the FeSO<sub>4</sub>.7H<sub>2</sub>O dose from 0.1 to 1 g. The color removal efficiency reached 98.43% during the first 5 minutes for 0.1 g of FeSO<sub>4</sub>.7H<sub>2</sub>O as seen in Fig. 10b. From the abovementioned results, the optimum FeSO<sub>4</sub>.7H<sub>2</sub>O dose is 0.1 g same as in case of using ZnO NPs. The results revealed that the degradation rate depends on the FeSO<sub>4</sub>.7H<sub>2</sub>O amount as reported by [44, 46]. It is also noticeable that the RB5 decolorization rate using photo-Fenton treatment is higher than using ZnO NPs treatment during the same photocatalytic time.

#### *Effect of initial RB5 dye concentrations*

The effect of initial RB5 dye concentrations on the photocatalytic efficiency using photo-Fenton was investigated as shown in Fig. 11. The degradation of RB5 dye was 99.76, 99.84, 99.84, 99.81, and 99.84 for the initial dye concentration of 50, 75, 100, 125 and 200 mg/L using FeSO<sub>4</sub>.7H<sub>2</sub>O<sub>2</sub>/UV. These results prove the photo-Fenton high efficiency with different RB5 initial concentrations. The high decolorization at the first 5 minutes for all dye concentrations may be attributed to the same dose of H<sub>2</sub>O<sub>2</sub> (1 ml) which may accelerate the production of  $\cdot\text{OH}$ . Trovo et al., [47], mentioned that the insufficient

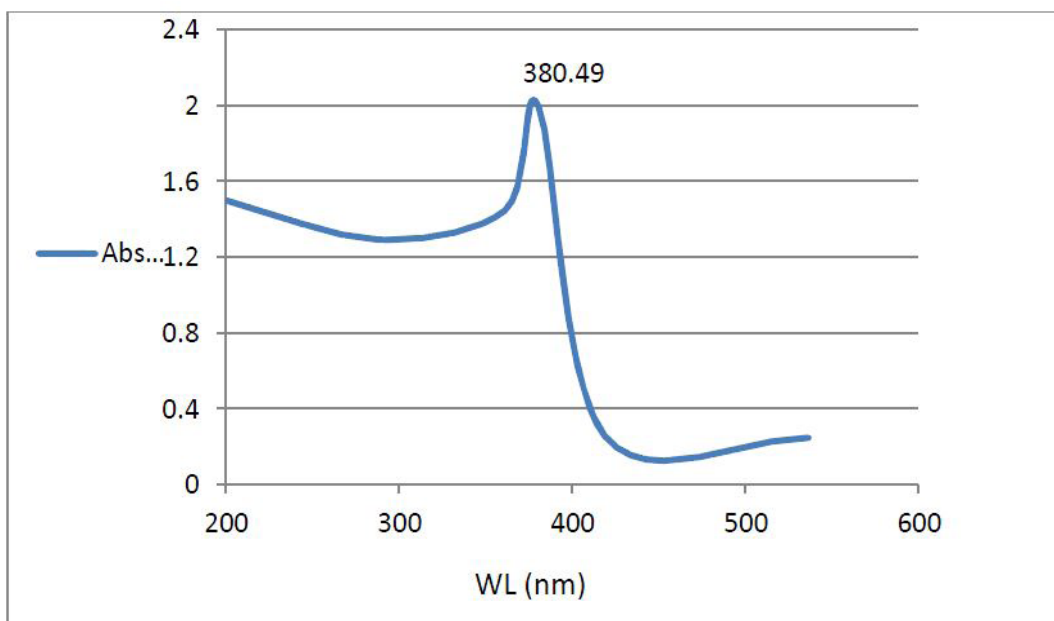


Fig. 7. UV-vis spectrum of chemically synthesized ZnO NPs.

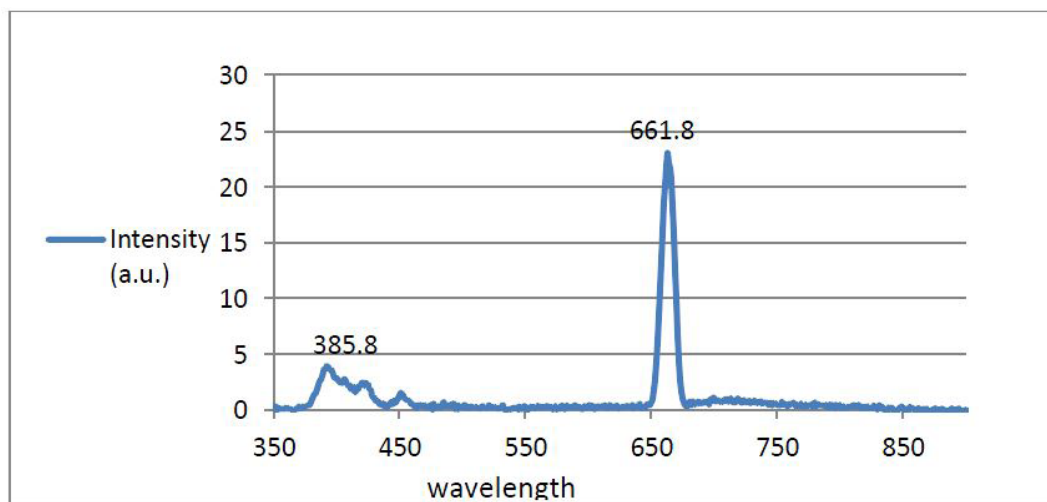


Fig. 8. photoluminescence spectrum of chemically synthesized ZnO NPs.

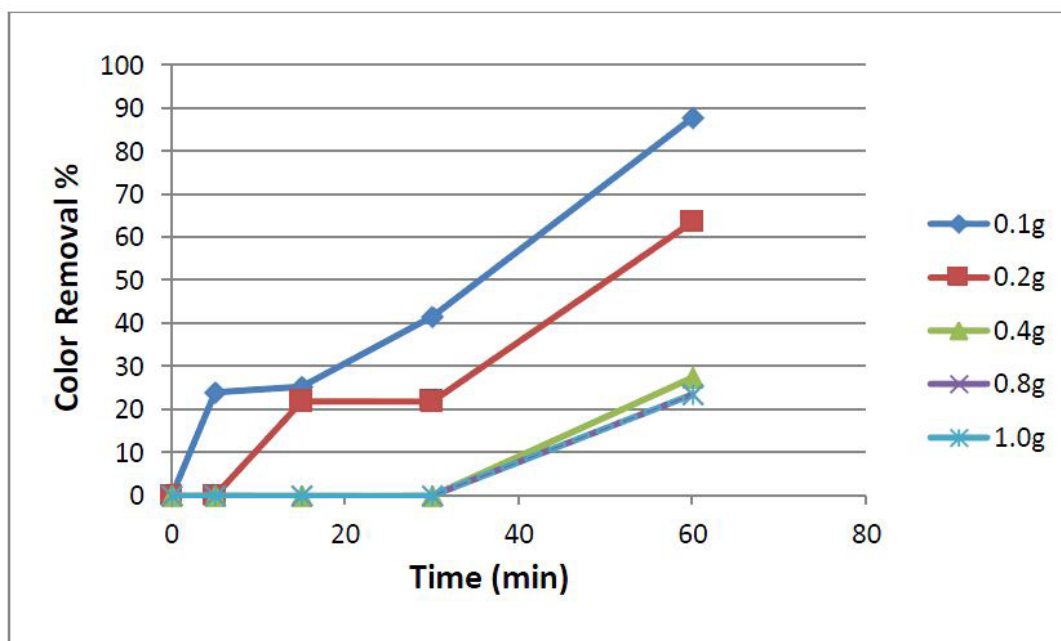


Fig. 9a. Effect of different ZnO catalyst dose on photocatalytic degradation of RB5 during the first 1h photocatalytic process at pH=7 and 1 ml of H<sub>2</sub>O<sub>2</sub> (35%).

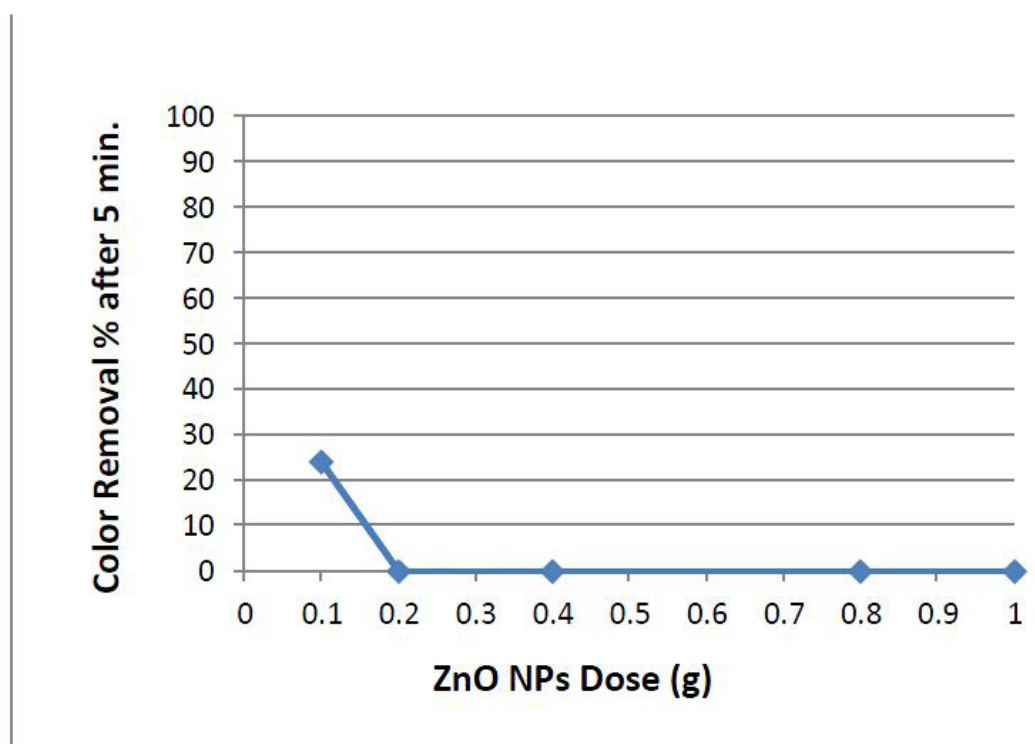


Fig. 9b. Effect of different ZnO catalyst dose on photocatalytic degradation of RB5 at pH=7 and 1 ml of H<sub>2</sub>O<sub>2</sub> (35%) after the first 5 minutes.

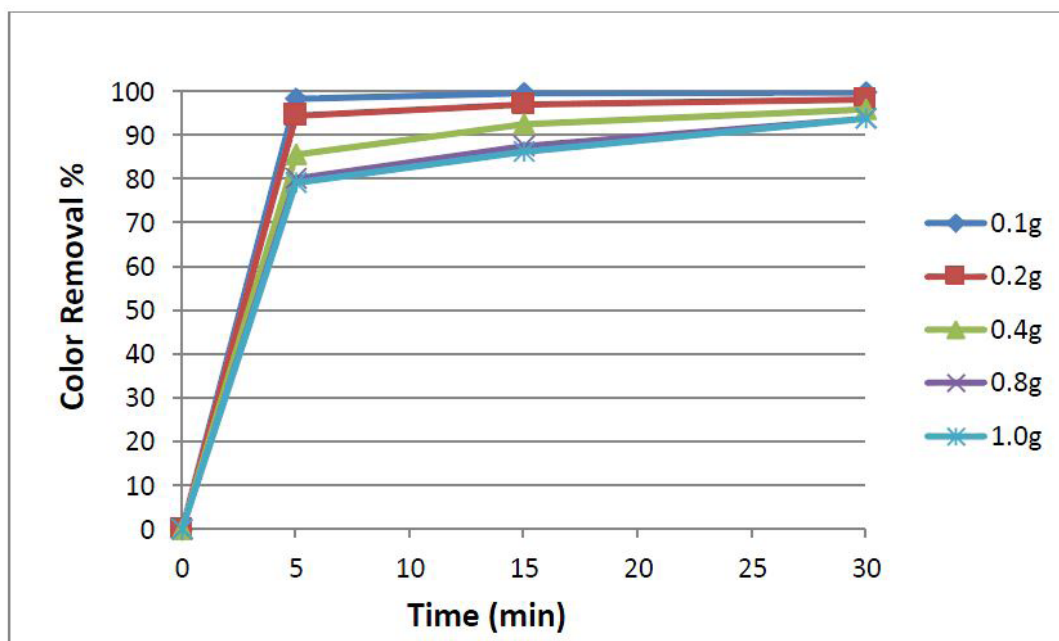


Fig. 10a. Effect of different  $\text{FeSO}_4 \cdot 7\text{H}_2\text{O}$  catalyst dose on photocatalytic degradation of RB5 at pH=7 and 1 ml of  $\text{H}_2\text{O}_2$  (35%).

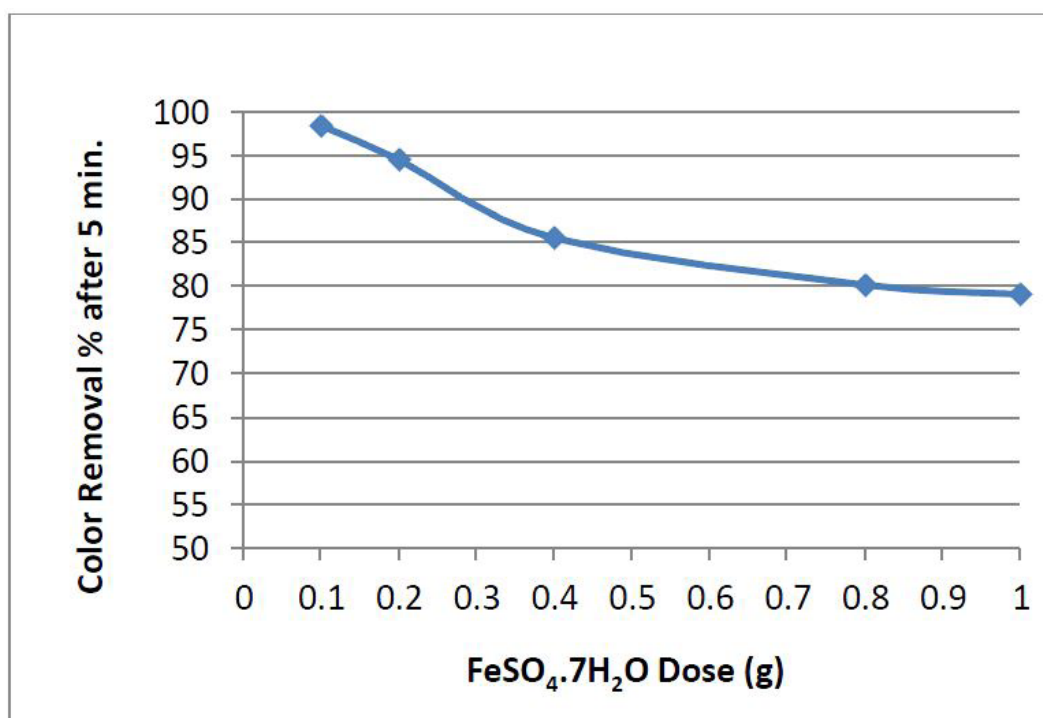


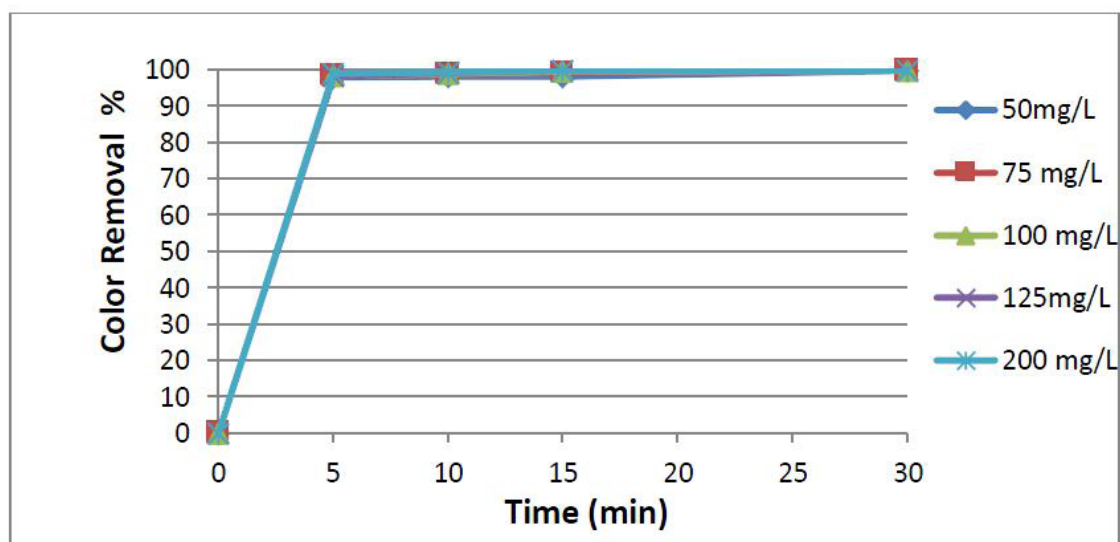
Fig. 10b. Effect of different  $\text{FeSO}_4 \cdot 7\text{H}_2\text{O}$  catalyst dose on photocatalytic degradation of RB5 at pH=7 and 1 ml of  $\text{H}_2\text{O}_2$  (35%) and after the first 5 minutes.

TABLE 1. The calculated crystal size of chemically synthesized ZnO NPs

Chemical ZnO NPs	
Position, °	Crystal Size [nm]
31.67	3.4
34.31	3.6
36.15	3.3
47.46	3.1
56.54	3.0
62.79	2.6
66.34	3.2
67.89	2.5
69.02	2.6
76.89	3.3

TABLE 2. The correlation coefficients ( $R^2$ ) for different initial concentrations of RB5 dye (by using 0.1 g of  $\text{FeSO}_4 \cdot 7\text{H}_2\text{O}$ ) at pH=7 and 1 ml of  $\text{H}_2\text{O}_2$  (35%) under UV irradiation.

Initial RB5 concentration (mg/L)	pseudo-first-order	pseudo-second-order
	$R^2$	$R^2$
50	0.79	0.79
75	0.72	0.86
100	0.65	0.95
125	0.53	0.90
150	0.48	0.81

Fig. 11. Effect of initial concentrations of RB5 on the photocatalytic degradation (by using 0.1 g of  $\text{FeSO}_4 \cdot 7\text{H}_2\text{O}$ ) at pH=7 and 1 ml of  $\text{H}_2\text{O}_2$  (35%) under UV irradiation.

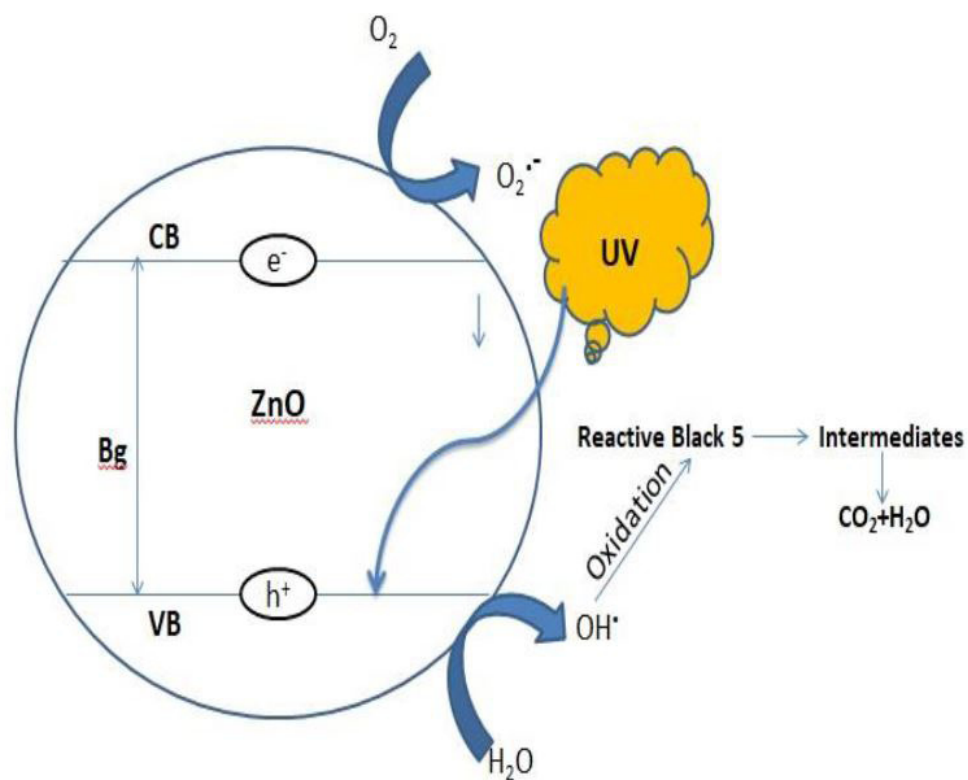


Fig. 12. Photo-induced formation mechanism of electron-hole pair in semiconductor ZnO particles with the presence of RB5 dye.

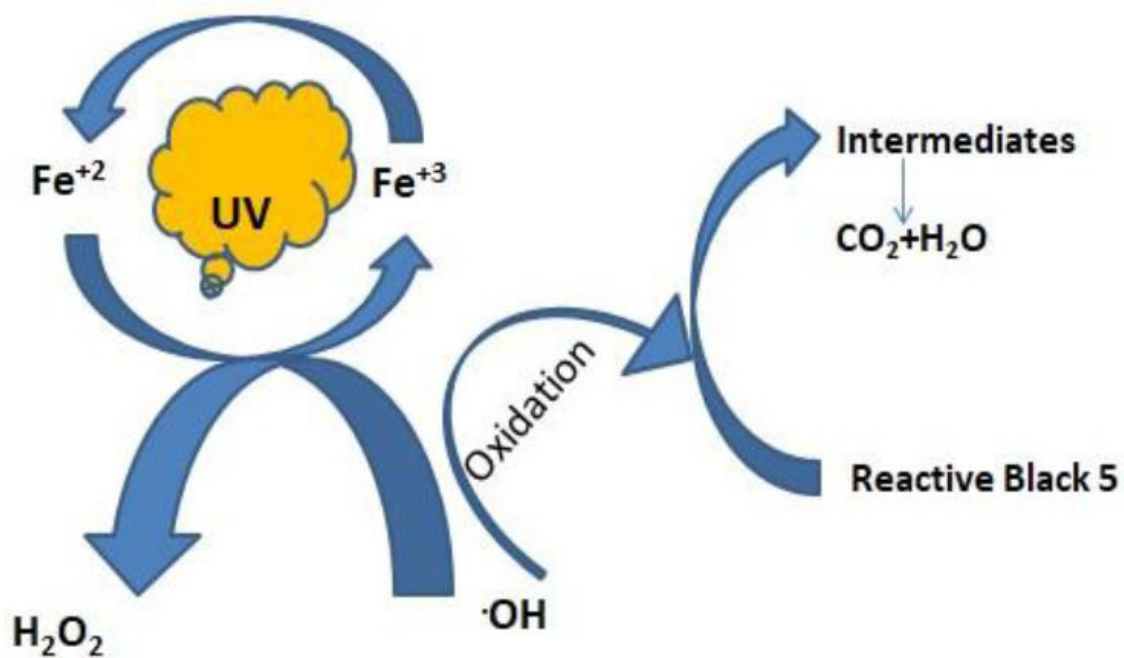


Fig. 13. Photo-Fenton oxidation mechanism for RB5 dye

amount of  $\text{H}_2\text{O}_2$  could not provide a sufficient amount of hydroxyl radicals for the maximal oxidative power.

#### *Kinetic study of photocatalytic degradation.*

The kinetics describes the photocatalytic degradation rate and provides valuable information about the reaction pathway and mechanism. The kinetic of RB5 photocatalytic degradation is analyzed using simulation of pseudo-first-order and pseudo-second-order (at different RB5 initial concentrations using 0.1 g of  $\text{FeSO}_4 \cdot 7\text{H}_2\text{O}$  at pH=7 and 1 ml of  $\text{H}_2\text{O}_2$  (35%) under UV irradiation). The identification between the models' calculated values and the experimental data is expressed by  $R^2$ ; the correlation coefficients as shown in Table 2. The high  $R^2$  values indicate that the RB5 photocatalytic degradation successfully follows the pseudo-second-order.

#### *Proposed mechanism of the RB5 degradation using ZnO NPs and photo-Fenton*

##### *ZnO NPs*

As shown in Fig. 12, the activation energy of the ZnO, which is the semiconductor particulate material, plays the key role of the heterogeneous photocatalysis process. By the action of energy with a suitable wavelength, this activation is reached with the absorption of photons by the semiconductor particle possessing sufficient energy to encourage the conduction of an electron ( $e^-$ ) from its valence band (VB) to the conduction band (CB), creating holes in the valence band ( $h^+$ ) that operate as oxidizing sites [48-51].

##### *Photo-Fenton*

In this process, Fe (II) is oxidized by  $\text{H}_2\text{O}_2$  to Fe (III), forming  $\cdot\text{OH}$  and  $\text{OH}^-$ . Fe (III) is then reduced back to Fe (II) by another molecule of  $\text{H}_2\text{O}_2$ , forming a hydroperoxyl radical and  $\text{H}^+$ . The net effect is a disproportionation of  $\text{H}_2\text{O}_2$  to create two different oxygen-radical species, with water ( $\text{H}^+ + \text{OH}^-$ ) as a byproduct.  $\cdot\text{OH}$  has a higher oxidizing potential and also, are non-selective for attacking the RB5 dye, leading to decolorization of RB5. The RB5 oxidation by  $\cdot\text{OH}$  produce some little fragments of intermediates organic compounds such as ketones, epoxides, aldehydes as reported by [14, 15] which may finally degraded to  $\text{CO}_2$  and  $\text{H}_2\text{O}$ .

The enhanced RB5 degradation using photo-Fenton treatment than ZnO NPs treatment may be

due to generating of more hydroxyl radicals under UV irradiation, according to Eqs. 1 - 4 [52-54].

#### **Conclusion**

In this study, the ZnO NPs synthesis was confirmed by FTIR, XRD and UV-vis analyses. According to TEM analysis, the chemically synthesized ZnO NPs have a particle size ranges from 19.1 nm and 33.1 nm. The UV-vis absorbance spectrum shows the presence of a strong and sharp peak at 380.49 nm that corresponds to the band gap of 3.25 which confirmed the synthesis of ZnO NPs. In this work, applied UV-based AOPs such as UV/ZnO and photo-Fenton for degradation of RB5 were compared on the basis of decolorization. Complete decolorization of RB5 solution (99.84%) was achieved only by photo-Fenton process throughout the complete range of all investigated parameters.

#### **Conflicts of Interest**

The authors declare no conflict of interest.

#### **References**

- Demiral H. and Güngör C., Adsorption of copper (II) from aqueous solutions on activated carbon prepared from grape bagasse. *Journal of Cleaner Production*, 124, pp.103-113 (2016).
- Ali R.M., Hamad H.A., Hussein M.M. and Malash, G.F., Potential of using green adsorbent of heavy metal removal from aqueous solutions: adsorption kinetics, isotherm, thermodynamic, mechanism and economic analysis. *Ecological Engineering*, 91, 317-332 (2016).
- Mills-Knapp S., Traore K., Ericson B., Keith J., Hanrahan D. and Caravanos J., *The World's worst pollution problems: assessing health risks at hazardous waste sites*. Blacksmith Institute, New York (2012).
- Sheng H.L. and Ming L.C., Treatment of textile wastewater by chemical methods for reuse. *Water Res*; 31(4):868-876 (1997).
- Chen T.Y., Kao C.M., Hong, A., Lin, C.E. and Liang, S.H., Application of ozone on the decolorization of reactive dyes-Orange-13 and Blue-19. *Desalination*, 249(3), 1238-1242 (2009).
- Tocchi C., Federici E., Fidati L., Manzi R., Vincigurerra V., and Petruccioli M., Aerobic treatment of dairy wastewater in an industrial three-reactor plant: Effect of aeration regime on performances and on protozoan and bacterial communities. *water research*, 46(10), 3334-3344 (2012).

7. Hassaan M.A. Advanced oxidation processes of some organic pollutants in fresh and seawater. PhD, A Thesis, Faculty of Science, Port Said University (2016).
8. Wang L., Yuan X., Zhong H., Wang H., Wu Z., Chen X. and Zeng G., Release behavior of heavy metals during treatment of dredged sediment by microwave-assisted hydrogen peroxide oxidation. *Chemical Engineering Journal*, 258, 334-340 (2014).
9. Xu H., Li M., Wang H., Miao J. and Zou L., Fenton reagent oxidation and decolorizing reaction kinetics of reactive red SBE. *Energy Procedia*, 16, 58-64 (2012).
10. Murugesan K., Nam I.H., Kim Y.M. and Chang, Y.S., Decolorization of reactive dyes by a thermostable laccase produced by *Ganoderma lucidum* in solid state culture. *Enzyme and Microbial Technology*, 40(7), 1662-1672 (2007).
11. Torrades F., Garcia-Montano J., Garcia-Hortal J.A., Domenech X. and Peral J., Decolorization and mineralization of commercial reactive dyes under solar light assisted photo-Fenton conditions. *Solar Energy*, 77(5), 573-581(2004).
12. Yu R.F., Lin C.H., Chen H.W., Cheng W.P. and Kao M.C., Possible control approaches of the Electro-Fenton process for textile wastewater treatment using on-line monitoring of DO and ORP. *Chemical engineering journal*, 218, 341-349 (2013).
13. El Nemr A., Hassaan M.A. and Madkour F.F., Advanced Oxidation Process (AOP) for Detoxification of Acid Red 17 Dye Solution and Degradation Mechanism. *Environmental Processes*, 5(1), 95-113 (2018).
14. Hassaan M.A., El Nemr A. and Madkour F.F., Testing the advanced oxidation processes on the degradation of Direct Blue 86 dye in wastewater. *The Egyptian Journal of Aquatic Research*, 43(1), 11-19 (2017).
15. El Nemr A., Hassaan M.A. and Madkour F.F., HPLC-MS/MS Mechanistic Study of Direct Yellow 12 dye Degradation Using Ultraviolet Assisted Ozone Process. *Journal of Water and Environmental Nanotechnology*, 3(1), 1-11(2018).
16. Lucas M.S. and Peres J.A., Decolorization of the azo dye Reactive Black 5 by Fenton and photo-Fenton oxidation. *Dyes and Pigments*, 71(3), 236-244 (2006).
17. Garcia J.C., Oliveira J.L., Silva A.E.C., Oliveira C.C., Nozaki J. and De Souza N.E., Comparative study of the degradation of real textile effluents by photocatalytic reactions involving UV/TiO<sub>2</sub>/H<sub>2</sub>O<sub>2</sub> and UV/Fe<sup>2+</sup>/H<sub>2</sub>O<sub>2</sub> systems. *Journal of hazardous materials*, 147(1-2), 105-110 (2007).
18. Uygur A. and K k E., Decolorisation treatments of azo dye waste waters including dichlorotriazinyl reactive groups by using advanced oxidation method. *Coloration Technology*, 115(11), 350-354 (1999).
19. Ay F., Catalkaya E.C. and Kargi F., A statistical experiment design approach for advanced oxidation of Direct Red azo-dye by photo-Fenton treatment. *Journal of Hazardous Materials*, 162(1), 230-236 (2009).
20. Ilha C.E., dos Santos A.J. and SouzaDe J.R., Degradation of Monoazo Pigments Red 53: 1 and Red 48: 2 by Fenton, Photo-Fenton and UV/Peroxide Reactions. *CLEAN-Soil, Air, Water*, 37(10), 799-805 (2009).
21. Parlıt N.B. and Akten D., Application of Box-Wilson experimental design method for the solar photocatalytic degradation of textile dyestuff with Fe (III)/H<sub>2</sub>O<sub>2</sub>/solar UV process. *Desalination*, 260(1-3), 193-198 (2010).
22. Torrades F. and Garcia-Montano J., Using central composite experimental design to optimize the degradation of real dye wastewater by Fenton and photo-Fenton reactions. *Dyes and pigments*, 100, 184-189 (2014).
23. Hermosilla D., Cortijo M. and Huang, C.P., The role of iron on the degradation and mineralization of organic compounds using conventional Fenton and photo-Fenton processes. *Chemical Engineering Journal*, 155(3), 637-646 (2009).
24. Masomboon N., Chen C.W., Anotai J. and Lu M.C., A statistical experimental design to determine o-toluidine degradation by the photo-Fenton process. *Chemical Engineering Journal*, 159(1-3), 116-122 (2010).
25. Silva M.R., Vilegas W., Zanoni M.V.B. and Nogueira R.F.P., Photo-Fenton degradation of the herbicide tebuthiuron under solar irradiation: Iron complexation and initial intermediates. *Water research*, 44(12), 3745-3753 (2010).
26. Ay F. and Kargi F., Advanced oxidation of amoxicillin by Fenton's reagent treatment. *Journal of hazardous materials*, 179(1-3), 622-627(2010).
27. Mendez-Arriaga F., Esplugas S. and Gimenez J., Degradation of the emerging contaminant ibuprofen in water by photo-Fenton. *Water research*, 44(2), 589-595 (2010).
28. Michael I., Hapeshi E., Michael C. and Fatta-Kassinos D., Solar Fenton and solar TiO<sub>2</sub> catalytic treatment of ofloxacin in secondary treated

- effluents: evaluation of operational and kinetic parameters. *Water research*, 44(18), 5450-5462 (2010).
29. Wahab R., Kim Y.S., Lee D.S., Seo J.M. and Shin H.S., Controlled synthesis of zinc oxide nanoneedles and their transformation to microflowers. *Science of Advanced Materials*, 2(1), 35-42 (2010).
  30. Soliman E.A., Elkatory M.R., Hashem A.I. and Ibrahim H.S., Synthesis and performance of maleic anhydride copolymers with alkyl linoleate or tetra-esters as pour point depressants for waxy crude oil. *Fuel*, 211, 535-547 (2018).
  31. Kaschner A., Haboeck U., Strassburg M., Kaczmarczyk G., Hoffmann, A. and Meyer B.K., Nitrogen-related local vibrational modes in ZnO: N. *Applied Physics Letters*, 80(11), 1909-1911 (2002).
  32. Nakamoto K., *Infrared spectra of inorganic and coordination compounds*, Wiley, New York (1997).
  33. [33] Li Z., Hou B., Xu Y., Wu D., Sun Y., Hu W. and Deng F., Comparative study of sol-gel-hydrothermal and sol-gel synthesis of titania-silica composite nanoparticles. *Journal of Solid State Chemistry*, 178(5), 1395-1405 (2005).
  34. Cullity B.D., *Elements of X-Ray Diffraction*, Addison-Wesley, Reading, Mass, USA, (1978).
  35. Dobrucka R. and Długaszewska J., Biosynthesis and antibacterial activity of ZnO nanoparticles using *Trifolium pratense* flower extract. *Saudi journal of biological sciences*, 23(4), 517-523 (2016).
  36. Tiwary P., Mahapatra R. and Chakraborty A.K., ZnO nanobristles prepared by one-step thermal decomposition of zinc nitrate as ultra-high response ethanol sensor at room temperature. *Journal of Materials Science: Materials in Electronics*, 30(6), 5464-5469 (2019).
  37. Yu J., Shan C.X., Qiao Q., Xie X.H., Wang S.P., Zhang Z.Z. and Shen D.Z., Enhanced responsivity of photodetectors realized via impact ionization. *Sensors*, 12(2), 1280-1287 (2012)..
  38. Song S., Tu J., He Z., Hong F., Liu W. and Chen J. Visible light-driven iodine-doped titanium dioxide nanotubes prepared by hydrothermal process and post-calcination. *Applied Catalysis A: General*, 378(2), 169-174 (2010).
  39. Kumar V., Swart H.C., Gohain M., Kumar V., Som S., Bezuindenhoudt B.C.B. and Ntwaeaborwa O.M., Influence of ultrasonication times on the tunable colour emission of ZnO nanophosphors for lighting applications. *Ultrasonics sonochemistry*, 21(4), 1549-1556 (2014).
  40. Jin X., Götz M., Wille S., Mishra Y.K., Adelung R. and Zollfrank C., A novel concept for self-reporting materials: stress sensitive photoluminescence in ZnO tetrapod filled elastomers. *Advanced Materials*, 25(9), 1342-1347 (2013).
  41. Kumar V., Gohain M., Som S., Kumar V., Bezuindenhoudt, B.C.B. and Swart H.C.m., Microwave assisted synthesis of ZnO nanoparticles for lighting and dye removal application. *Physica B: Condensed Matter*, 480, 36-41(2016).
  42. Ahmad M.Z., Qureshi K., Bhatti I.A., Zahid M., Nisar J., Iqbal M. and Abbas M., Hydrothermal synthesis of molybdenum trioxide, characterization and photocatalytic activity. *Materials Research Bulletin*, 100, 120-130 (2018).
  43. Ashar A., Iqbal M., Bhatti I.A., Ahmad M.Z., Qureshi K., Nisar J. and Bukhari I.H., Synthesis, characterization and photocatalytic activity of ZnO flower and pseudo-sphere: Nonylphenol ethoxylate degradation under UV and solar irradiation. *Journal of Alloys and Compounds*, 678, 126-136 (2016)..
  44. Galindo C., Jacques P. and Kalt A., Photooxidation of the phenylazonaphthol AO20 on TiO<sub>2</sub>: kinetic and mechanistic investigations. *Chemosphere*, 45(6-7), 997-1005 (2001).
  45. Hassaan M.A., El Nemr A. and Madkour F.F., Advanced oxidation processes of Mordant Violet 40 dye in freshwater and seawater. *The Egyptian Journal of Aquatic Research*, 43(1), 1-9 (2017).
  46. Shaban M., Abukhadra M.R., Ibrahim S.S. and Shahien M.G., Photocatalytic degradation and photo-Fenton oxidation of Congo red dye pollutants in water using natural chromite—response surface optimization. *Applied Water Science*, 7(8), 4743-4756 (2017).
  47. Trovó A.G., Hassan A.K., Sillanpää M. and Tang W. Z., Degradation of Acid Blue 161 by Fenton and photo-Fenton processes. *International journal of environmental science and technology*, 13(1), 147-158 (2016).
  48. Serpone N., Relative photonic efficiencies and quantum yields in heterogeneous photocatalysis. *Journal of Photochemistry and Photobiology A: Chemistry*, 104(1-3), 1-12 (1997).
  49. Sichel C., Blanco J., Malato S. and Fernandez-Ibanez P., Effects of experimental conditions on *E. coli* survival during solar photocatalytic water disinfection. *Journal of Photochemistry and photobiology A: Chemistry*, 189(2-3), 239-246 (2007).

50. Fujishima A., Zhang X. and Tryk D.A., Heterogeneous photocatalysis: from water photolysis to applications in environmental cleanup. *International journal of hydrogen energy*, 32(14), 2664-2672 (2007).
51. Amirante R., Demastro G., Distaso E., Hassaan M.A., Mormando A., Pantaleo A.M. and Clodoveo, M. L., Effects of Ultrasound and Green Synthesis ZnO Nanoparticles on Biogas Production from Olive Pomace. *Energy Procedia*, 148, 940-947 (2018).
52. Huang Y.H., Huang Y.F., Chang, P.S. and Chen C.Y., Comparative study of oxidation of dye- Reactive Black B by different advanced oxidation processes: Fenton, electro-Fenton and photo-Fenton. *Journal of hazardous materials*, 154(1-3), 655-662 (2008).
53. Iqbal M. and Bhatti I.A., Gamma radiation/ H<sub>2</sub>O<sub>2</sub> treatment of a nonylphenol ethoxylates: degradation, cytotoxicity, and mutagenicity evaluation. *Journal of hazardous materials*, 299, 351-360 (2015).
54. Iqbal M., Abbas M., Arshad M., Hussain T., Ullah Khan A., Masood N. and Ahmad Khera R., Short Communication Gamma Radiation Treatment for Reducing Cytotoxicity and Mutagenicity in Industrial Wastewater. *Polish Journal of Environmental Studies*, 24(6), 2745-2750 (2015).

## التحلل الضوئي لصبغة RB5 باستخدام تقنيته الفوتوفنتون و جزيئات أكسيد الزنك النانوية تحت الأشعة فوق البنفسجية

محمد علي حسان<sup>1</sup>، مروة رمضان القاطوري<sup>2</sup>، رحاب محمد علي<sup>2</sup> و أحمد النمر<sup>1</sup>

<sup>1</sup> شعبة البيئه البحرية، المعهد القومي لعلوم البحار والمصايد، الاسكندرية، مصر.

<sup>2</sup> معهد التكنولوجيا المتقدمة و المواد الجديدة، مدينة الابحاث العلمية و التطبيقات التكنولوجية، مدينة برج العرب الجديدة، الاسكندرية، مصر.

في هذه الدراسة ، تم تأكيد تخليق جزيئات اكسيد الزنك النانويه من خلال تحليلات FTIR و XRD و UV-vis. وفقاً لتحليل TEM فإن اكسيد الزنك المحضر كيميائياً يتراوح حجم جسيماته بين 1.91 نانومتر و 1.33 نانومتر. يُظهر طيف الامتصاص بالأشعة فوق البنفسجية وجود قمة قوية وحادة عند 94.083 نانومتر والتي تتوافق مع فجوة النطاق 52.3 والتي أكدت تخليق اكسيد الزنك. في هذا العمل ايضا ، تمت مقارنة عمليات الاكسده المتقدمه المستندة إلى الأشعة فوق البنفسجية مثل ZnO/UV و photo-Fenton لتكسير صبغه RB5 على أساس إزالة اللون. تم تحقيق إزالة اللون الكامل لصبغه RB5 حوالى (99.84%) فقط من خلال عملية photo-Fenton.